EUROPEAN FUSION DEVELOPMENT AGREEMENT

EFDA–JET–PR(02)08

V.I. Afanasyev and A. Gondhalekar et al

A Neutral Particle Analyzer/Isotope Separator for Measurement of Hydrogen Isotope Composition of JET Plasmas

A Neutral Particle Analyzer/Isotope Separator for Measurement of Hydrogen Isotope Composition of JET Plasmas

V.I. Afanasyev[1], A. Gondhalekar, P.Yu. Babenko[1], P. Beaumont, P. De Antonis, A.V. Detch[1], A.I. Kislyakov[1], S.S. Kozlovskij[2], M.I. Mironov[1], M.P. Petrov[1], S.Ya. Petrov[1], F.V. Tschernyshev[1], C.H. Wilson, and contributors to the EFDA-JET workprogramme*

UKAEA/Euratom Fusion Association, Culham Science Centre, Abingdon, OX14 3DB, UK
[1]A.F. Ioffe Physical-Technical Institute, 194021 St. Petersburg, Russia
[2]St. Petersburg Technical University, St. Petersburg, Russia
** See annex of J. Pamela et al, "Overview of Recent JET Results and Future Perspectives", Fusion Energy 2000 (Proc. 18th Int. Conf. Sorrento, 2000), IAEA, Vienna (2001).*

Submitted for publication in Review of Scientific Instruments

ABSTRACT

This paper describes a Neutral Particle Analyzer/Isotope Separator(ISEP) developed for measurement of relative hydrogen isotope composition of JET plasmas. The ISEP deployed on JET can be regarded as a prototype of an instrument proposed for measurement of spatial profile of ratio of density of deuterium and tritium ions in the plasma, $n_D(r)/n_T(r)$, in the International Thermonuclear Experimental Reactor (ITER). ISEP makes simultaneous measurements of energy distribution of efflux of hydrogen isotope atoms (H, D and T) from the plasma. From such measurements it is possible to deduce the radial profile of relative hydrogen isotope ion composition of the plasma, and radial transport of ions of one isotope across plasma of another isotope species.

The main elements of the ISEP are: a) stripping of atoms in a thin carbon foil to produce secondary ions, b) acceleration of secondary ions, c) E//B analysis of the secondary ions in specially designed non-uniform magnetic and electric fields, d) counting of energy and mass analyzed secondary ions using detectors consisting of thin($1 \leq t(\mu m) \leq 7$) CsI(Tl) scintillators deposited directly on miniature photo-multiplier tubes(PMT) mounted in vacuum. The ISEP has high contrast between atoms of neighbouring masses($\geq 10^3$ for $E \approx 5$keV, and much greater at higher energies), and high detection efficiency ($0.06 \leq \varepsilon \leq 0.83$ for atoms of $5 \leq E(keV) \leq 150$). The ISEP detectors have very low sensitivity for neutron and γ-ray radiation ($\leq 10^{-7}$ of ion detection efficiency). This makes possible reliable use of ISEP with deuterium-tritium (D-T) plasmas in JET and ITER using only modest amount of shielding. First results of the use of ISEP on JET, demonstrating capabilities of this instrument for determination of H-D composition of plasmas, are also presented in this paper.

1. INTRODUCTION

An important measurement objective in nuclear fusion devices is to determine the radial profile of hydrogen isotope composition of the plasma. Such measurements are required for many reasons. First, to get the optimal regime of ignition and fusion burn, it is necessary to achieve the optimal D-T density ratio in the plasma. Thus, from the perspective of obtaining the most effective fusion burn regime, the D-T density ratio in the plasma core is one of the most important parameters to be measured and controlled in any fusion reactor. Second, there is a requirement to study energy confinement scaling in plasmas with different hydrogen isotope (H, D, T) composition. Analysis of energy transport in tokamaks has shown that the energy confinement time τ_E depends on the hydrogen isotope composition. This effect was first studied in detail in ASDEX [1], where it was shown that τ_E was larger in deuterium than in hydrogen plasmas, and the authors conjectured further improvement in D-T plasmas. Subsequent experiments with D-T plasmas in large tokamaks, TFTR [2,3] and JET [4,5], showed that other plasma behaviour also depends on the hydrogen isotope composition. In TFTR it was found that τ_E increased with increasing tritium fraction in D-T plasmas, while this effect failed to reproduce in JET. On the other hand D-T experiments in JET showed that increased tritium concentration yielded lower power threshold for transition to the H-mode.

An important measurement deficiency during the deuterium-tritium fusion experiments in JET

and TFTR has been the absence of measurement of the hydrogen isotope composition of the plasma in the central region. The isotope composition was estimated from the relative amounts of deuterium and tritium neutral beam injection(NBI) into the plasma. This approximate approach gave rise to many uncertainties in (a) energy transport analysis due to the possibility of ion mass dependence of local thermal transport coefficients, (b) analysis of α-particle heating of electrons, due to the possibility of an isotope effect on energy transport as mentioned above, (c) computation of equilibration power to the electrons from α-particles and hotter plasma fuel ions, and (d) analysis of ion cyclotron resonance frequency(ICRF) heating of plasmas with multiple hydrogen isotope ions in simultaneous resonance, where the wave dispersion and power sharing between different ions depends on plasma composition. ICRF heating and current drive experiments relying on mode conversion will suffer more.

These interpretation deficiencies can be addressed only by measurement of H/D/T ion density ratio inside the plasma, with spatial resolution, and for a wide range of values of the ratio. A method for achieving this objective using a neutral particle analyzer(NPA)was analyzed for JET[6]. This is the only method available at present, it relies on analysis of efflux of H, D and T atoms from the plasma. The efflux in the energy range $0 \leq E(keV) \leq 150$ is produced by charge-exchange (CX) reactions between plasma ions and thermal hydrogen isotope atoms present in the plasma. In D-T plasmas one- and two-electron species of helium will also be effective electron donors in CX reactions. In the energy range $E(MeV) \geq 0.3$ one- and two-electron species of intrinsic plasma impurity ions become dominant in JET[7]. The rate of production of CX atoms at any point in the plasma is given by $n_H \Sigma (n_{DO} \langle \sigma \upsilon \rangle)_j$, where n_H is density of hydrogen isotope (H,D,T) ions, n_{DO} is the density of electron donors which include hydrogen, helium and impurity species, $\langle \sigma \upsilon \rangle$ is appropriately averaged rate-coefficient for CX reaction, and the sum is over all donor species j. On the way out of the plasma the atomic flux is attenuated, due to ionisation by charge-exchange and collisions with plasma ions and electrons. For different hydrogen isotope atoms in the same plasma, the total attenuation coefficient depends only on the speed of the exiting atoms [6], and therefore the magnitude of relative hydrogen isotope atom production inside the plasma is reliably scaleable from the measured efflux outside the plasma. Lastly, corresponding to the energy of the detected atoms there exists a spatial emissivity profile $\boldsymbol{\varepsilon}(r,E)$ which is fully explained in ref.[6]. $\boldsymbol{\varepsilon}(r,E)$ can be understood as giving, as a function of distance along the line-of-sight, the normalized probability that the measured atomic flux of given energy originated at that spatial location. Thus, by measuring the energy distribution of efflux of the different hydrogen isotope atoms, it is possible to deduce the spatial distribution of relative hydrogen isotope ion density in the plasma. Calculations for JET plasmas[6] show that in the range of plasma parameters and attenuation coefficients usually obtained in JET, in order that H, D and T atoms with $\boldsymbol{\varepsilon}(r,E)$ peaked in the plasma core are observed, it is necessary to measure the atomic efflux in the energy range $E = (5 — 10)T_i$, where T_i is the average plasma ion temperature. Tests of this method were carried out on JET using an existing time-of-flight(TOF) NPA[6], which showed that the available conventional NPAs were not adequate for

achieving the above measurement objective in JET, and a superior NPA instrument was required having a wider energy range, greater sensitivity to efflux of H/D/T atoms, greater mass separation, and greater discrimination against neutron and γ-ray induced noise signal.

In this paper we describe a new NPA/Isotope Separator (ISEP) developed for determining the H/D/T isotope composition of JET plasmas. ISEP is designed for high mass separation, giving contrast of $\geq 10^3$ in measuring neighbouring hydrogen isotopes. ISEP also has high detection efficiency, close to 100% at the highest energies. The ISEP detectors have high sensitivity for hydrogen isotope ions (~1) and simultaneously very low sensitivity for neutron and γ-ray radiation ($\leq 10^{-7}$). Laboratory tests (described later in the paper) of detectors give the result that it may be feasible to use ISEP in JET DT experiments, with neutron yield of $\leq 2 \times 10^{18}$ n/s, without any shielding. In this paper we present also first results of application of ISEP on JET, demonstrating capabilities of the instrument in studies of deuterium plasma.

2. DESIGN AND OPERATIONAL PRINCIPLES OF ISEP

The ISEP is an instrument designed to measure absolute energy distribution of efflux of H, D and T atoms emitted by fusion plasmas, in the energy range 5-740 keV for H^0, 5-370 keV for D^0, and 5-250 keV for T^0. The fluxes of H^0, D^0 and T^0 are measured simultaneously, with mass-suppression of neighbouring masses of $\geq 10^3$ for E≈5keV and much greater at the highest energies. Practically, this large mass-suppression enables measurement of minority isotope efflux, and therefore relative ion density, as low as 1%. We expect the ISEP to reliably measure the atomic fluxes from JET plasmas with neutron emission rate up to 2×10^{18} n/s, which corresponds to neutron flux of ~2×10^{10} n/(cm^2.s) at the location of the instrument, without shielding.

Special features of ISEP are: (a) stripping of atoms from the plasma using a thin carbon foil, eliminating conventional gas cell for stripping, (b) acceleration of secondary ions after stripping, by 0-100 kV, to increase detection efficiency and contrast between ions and neutron/γ-ray induced signals in the scintillator detectors, (c) E//B analysis of ions in specially designed non-uniform B and E fields, providing two dimensional focusing in the dispersion system, and therefore high contrast between neighbouring isotope atoms, (d) thin scintillators deposited on thin-window miniature PMTs installed in vacuum, giving very low sensitivity to neutron and γ-ray fluxes (a 100keV ion is detectable in a background of $\geq 10^7$ neutrons and γ-rays incident on the detector).

Fig. 1 shows the ISEP layout. It consists of three main sections, acceleration, magnet, and detector chambers. The acceleration chamber consists of an input aperture, a collimator slit mechanism, a removable calibration aid, a thin carbon stripping foil supported on a nickel mesh, and an output aperture. Elements of magnet and detector chambers are a light emission diode for detector testing, optical laser for alignment, Hall probe, magnet giving non-uniform field, electrostatic condenser giving non-uniform electric field, detector array. In fig.1 A^0 are incident atoms while A^+ are secondary ions. Acceleration voltage of U_{acc} = +0-100 kV is used, acceleration takes place in the gap between #4 and #5. Fig.2 shows the external view of the ISEP assembly, illustrating some details of the three

main chambers. The ISEP pumping system (not shown in the figure) is attached to port P. It is separated by aperture #1 from the beam-line with its independent pumping system. This differential pumping ensures that very high vacuum($\leq 10^{-8}$ mb) is maintained in the accelerator chamber while the beam-line and torus pressures fluctuate. Access, for removing the accelerator electrode and for exchanging the carbon foil, is obtained through port H.

2.1 THE ACCELERATOR CHAMBER FOR COLLIMATION, STRIPPING AND FOCUSING

The accelerator chamber incorporates a collimator/slit mechanism, accelerator unit with stripping foil and a 100kV vacuum feed-through. Referring to fig.1, the ISEP collimator consists of two fixed apertures, #1(ϕ = 2mm) at the entrance of the accelerator chamber and #5(ϕ = 8 mm) at the entrance of magnet chamber, separated by 431.4 mm. The intermediate slit mechanism (#2) gives a choice of one of three apertures of diameter of 0.2 mm, 0.7 mm or 2.0 mm. This can be used to control the flux into the ISEP. The positive electrode of the accelerator consists of a hollow polished stainless steel cylinder with 8mm apertures on axis at both ends. A 300≈, ϕ = 12mm carbon stripping foil is mounted inside the cylindrical electrode close to the exit end. A thin nickel mesh having 90% transmission supports the foil. A feed-through rod and two spring clamps hold the cylindrical acceleration electrode. For inspection and for exchanging the foil when necessary, the acceleration unit can be removed from the chamber by hand through the port H shown in fig.2. The secondary ions formed by the stripping foil are accelerated in the gap between the cylindrical electrode and aperture #5, which is at ground potential.

The need for secondary ion acceleration arises because the ion detectors, thin CsI(Tl) scintillators mounted on PMTs, developed for operation in a high neutron environment and presently employed in the high energy NPA [8], are not adequate for measurements in the range $10 \leq E(keV) \leq 100$ because of insufficient discrimination between ions and background neutrons/γ-rays. We increase the contrast between the detected ions and neutrons by adding up to ~100kV to the ions after secondary ionization in the foil, thereby increasing the detector response to the ions. Modeling of the detector response shows that acceleration voltage of 80 — 100 kV yields an increase of factor ~10^3 in the ion-signal/neutron-background ratio, giving reliable detection of $10 \leq E(keV) \leq 100$ hydrogen isotope atoms in high fusion yield DT plasmas in JET. This statement is examined in greater detail below in section 3.

2.2 THE MAGNET CHAMBER FOR E||B ELECTROMAGNETIC DISPERSION OF SECONDARY IONS

The magnet chamber incorporates the magnet body with the excitation coils, Hall probe, electromagnet poles, and an electrostatic analyzing condenser. The atoms entering the ISEP are collimated by the apertures #1, #2, and #5. After stripping by the foil and acceleration, the secondary ions are deflected by the magnet through 180^o. The gap between the magnet poles is not uniform, the shape of the gap is designed to give the best two-dimensional focusing of the ions entering the

electrostatic analyzer (see section 4). After momentum dispersion in the magnetic field the secondary ions traverse an electric field for mass separation. The condenser plates are of special two-dimensional shape designed to give optimal mass-separation of ions and simultaneously good collection of ions into the entrances of corresponding detectors. A Hall probe is installed in the magnet chamber (see Fig. 1) with the aim to measure and monitor directly the magnetic field inside the gap between magnet poles. An alignment laser and light emitting diode are attached to the viewing port of the ISEP. The light emitting diode serves as detector testing aid.

2.3 HIGH EFFICIENCY ISEP DETECTORS WITH LOW NEUTRON/G-RAY SENSITIVITY

The detector plane is transverse to the plane of the magnet gap. Ions with the same q/m (charge to mass ratio) intercept the detector plane at the same distance from the mid-plane of the magnet. Three groups of detectors are located in the detector plane, each group detecting ions of a different isotope of hydrogen (H, D and T). Thus the energy distribution of efflux of all three isotope atoms can be measured separately and simultaneously. Fig. 3 presents a map of detector positions in the detector plane. Here X is distance along the magnetic dispersion (giving ion energy separation), and Y is distance along the electric dispersion (giving ion mass separation). The ISEP is equipped with 32 individual detectors with accompanying preamplifier and ADC data acquisition electronics. 14 detectors are assigned to hydrogen, 10 to deuterium and 8 to tritium measurements.

The ISEP detectors consist of CsI(Tl) scintillators sputtered onto thin(0.5mm) quartz slides which are then optically glued to the thin entrance windows of Hamamatsu-R2248 PMTs. The scintillator is 8mm square, matching the PMT window. The scintillator thickness varies between $1 \leq t(\mu m) \leq 7$, each scintillator is designed to be thick enough only to fully stop the ions incident on it. In different detectors, as the energy of incident ions increases, the scintillator thickness is increased to match. The design provides simultaneously for maximal ion detection efficiency and low neutron/γ-ray sensitivity. The detectors are located in the focal plane of ion trajectories, mounted on a detector flange, which seals the detector chamber. To obtain the required energy and mass resolution in the low energy channels, diaphragms are installed at the entrances to the detectors . Each PMT is fitted with a magnetic shield made of μ-metal to reduce sensitivity to stray magnetic fields.

3. TESTS OF ISEP DETECTORS USING NEUTRON AND γ-RAY SOURCES

The aim of the laboratory tests was to qualify the neutron/γ-ray sensitivity of the detectors and measure their energy resolution, with the intent to model the signal-to-noise behavior of the detectors under conditions of intense neutron/γ-ray background. In JET DD plasma operation the fusion neutron yield is presently $\leq 5\times10^{16}\ s^{-1}$, giving a neutron flux at the location of ISEP detectors of $\leq 5\times10^{8}\ s^{-1}\ cm^{-2}$ with a maximum neutron energy of 2.5 MeV. Interaction with the surrounding materials produces γ-rays with a average energy of 1 MeV. In DT plasmas the neutron flux at the detectors is $\leq 5\times10^{10}\ s^{-1}\ cm^{-2}$, with maximum neutron energy of 14 MeV. As mentioned earlier, the

neutron/γ-ray sensitivity of the ISEP detectors has been reduced greatly by minimising the thickness of the scintillators, and by reducing the amount of glass incorporated in the detector/PMT assembly. The detectors are installed in vacuum inside the detector chamber to reduce all intermediate elements between the scintillator and PMT entrance window. The neutron/γ-ray sensitivity of the detectors has been measured using radioactive sources.

To simulate the background radiation of the high temperature plasma we have used a ^{252}Cf neutron source which generates neutrons with a continuous energy spectrum up to a maximum energy E ~ 10 MeV, the average energy of the neutrons is <E> = 2.2 MeV. The neutron emission is accompanied by γ-ray emissivity of 2.7 γ-rays/neutron, having average energy of ~1 MeV. This source simulates well the neutron and γ-ray environment of ISEP detectors in fusion plasma experiments. The source was installed near the input window of the detector and the amplitude distribution of signal pulses produced by the detector was measured. Fig.4 presents the results of the measurement in integral form. The X-axis denotes a detection threshold of pulses. It is calibrated in terms of the corresponding energy of H^+ ions. The Y-axis gives the ratio of the number of pulses counted with a pulse height greater than the detection threshold to the total number of neutrons and γ-rays incident on the detector.

The results are given for: a bare PMT(curve #1), a PMT with a thin 1.1μm scintillator (for the lowest energy ions)(curve #2), a PMT with a thick 7μm scintillator(for the highest energy)(curve #5), and PMTs with two intermediate thickness scintillators(curves #3 and #4). Fig.4 shows that the n/γ-ray sensitivity increases with scintillator thickness, and decreases by 2-3 orders of magnitude in going from E_H(keV)=10 to E_H(keV)=100. Since the detection efficiency of ions in the energy range of interest is close to 100%, this result gives the justification for acceleration of the ions before detection. Fig. 4 shows that by uniformly increasing the energy of all ions by acceleration through 80-100 kV, the signal-to-n/γ-ray background ratio can be increased by three orders of magnitude for low energy hydrogen ions and a little less for high energy ions, due to increased separation of amplitude of ion pulses from that of the n/γ-ray background.

A collimated beam of 5.5 MeV α-particles from a Pu^{238} source was used to measure the energy resolution of the ISEP detectors. The energy of the α-particles at the detector was reduced to 200 keV using a suitable air gap between the source and the detector. The output pulse height spectrum from all 32 detectors (scintillator/PMT combination) was measured. The energy resolution δE/E of the isolated detector was defined as the ratio of the full width at half maximum of the pulse height spectrum and the amplitude at the peak of the spectrum. The 32 ISEP detectors yield the result $0.35 \leq \delta E/E \leq 0.52$. Calibration of ISEP using variable energy H and D atomic beams (see section #5 below) showed that the energy width ΔE of the ISEP channels was much less than δE. This result shows that the energy resolution of the E||B electromagnetic analyzer is much greater than that of the detectors. In the analysis of atomic efflux discussed later in the paper only calibrations of ΔE/E using beams were used.

Combining the above ingredients allows development of a model of detector response, and to quantify the ability of ISEP detectors to count ions in the presence of intense n/γ-ray background

on JET. The result is illustrated by fig. 5. The figure presents a numerical code simulation of ISEP detector pulse height distribution when used to detect deuterium atoms in the presence of given DT neutron yield in JET. In the simulation deuterium atoms with energy E =5 keV enter the ISEP. Acceleration voltage U_{acc} = 80 kV is used (giving secondary ion energy E_D=85 keV), and D^+ count rate is 10^4/s. Simulation results are shown for four different levels of neutron yield from the plasma, ranging from 10^{17} to $5x10^{18}$ n/s. The last value is close to the highest DT fusion yield in JET, recorded in Pulse No: 42976 during the DTE1 experiments in 1997. In fig.5 the neutron flux at the ISEP detector location would be 10^9 to $5x10^{10}$ n/s cm^2.

Pulse pile-up effects of small n/γ-ray induced pulses are fundamental to consideration of ion detectability, these have been taken into account in the simulation. We have used the measured neutron sensitivity (fig. 4) and energy resolution δE of the detector. No neutron shielding of the detectors was incorporated in these calculations. It is seen that even with neutron yield of of 2.10^{18} n/s, D^+ ions can be clearly distinguished from neutron background, without any shielding. This conclusion extends to T^+ ions as well.

4. OPTIMIZATION OF THE ISEP ACCELERATION/DISPERSION SYSTEM

A key parameter of ISEP is the total detection efficiency for incident atoms. It is determined by stripping efficiency of the carbon foil, and by subsequent factors affecting secondary ion trajectories, namely: a) scattering of ions by the stripping foil, b) acceleration after stripping, c) effect of magnetic and electric fields of the dispersion system, d) efficiency of detectors. A design aim for ISEP was to obtain optimum detection efficiency. To this end we have performed experimental studies and numerical modelling of all factors listed above.

(a) Scattering of secondary ions after stripping

The angular scattering distribution of atoms passing through the stripping foil has to be properly taken into account in the ISEP design. It determines the subsequent geometrical layout of the analyzer and configuration of its electromagnetic dispersion system. Therefore this parameter was measured carefully. Measurements were performed using two calibration facilities with beams of H and D atoms, one operating in the energy range $5 \le E_H^0, {}_D^0 (keV) \le 27$ and the other in $5 \le E_H^0 (keV) \le 230$. A carbon stripping foil of 300≈ thickness was used. The measured angular distribution of the secondary ions exiting from the stripping foil was found to be approximately Gaussian. The results are given in fig.6, where the parameter $\delta\phi_{scatt}$ describes the width of angular distribution of secondary ion intensity given by the expression $I(\delta\phi) \sim I(0)\exp\{-(\delta\phi)^2/(\delta\phi_{scatt})^2\}$.

Two important features were found, first that the variation of $\delta\phi_{scatt}$ with ion energy is close to $\sim E^{-1}$ dependence, and second that there is not a significant difference in scattering of H^+ and D^+ ions. Both these features are in agreement with theoretical predictions in ref.[9,10], enabling these measurements to be extrapolated to the higher energy range of the ISEP. In addition, because safety related restrictions precluded tritium atom beams, required scattering data for tritium was obtained from this validated numerical modelling (see section 5 on ISEP Calibration).

b) Focusing of secondary ions due to acceleration

H and D atomic beams with energy $5 \leq E_H^0, {}_D^0 (\text{keV}) \leq 27$ keV were used for adjusting the secondary ion focusing system to achieve minimal ion losses after stripping and acceleration. The focusing system shown in fig.7 is formed by the 8mm exit aperture of the accelerator unit at (+)HV and the 8mm entrance aperture (#5 in fig.1) to the magnet gap, at ground potential. The distance between the two apertures was adjusted and the optimal distance of 20mm found. Fig. 8 and fig.9 present H^+ ion intensity distributions, measured at the entrance to the analyzing magnet, in a direction perpendicular to the axis of acceleration in the plane of magnetic dispersion. Measurements were made using a movable 1mm diameter input aperture channeltron detector located at the entrance to the magnet. Fig.8 and fig.9 show the results for two settings of the accelerator, with $U_{acc} = 0$kV and $U_{acc} = 90$kV respectively.

These measurements show that acceleration after stripping has the beneficial effect of narrowing the spatial distribution of secondary ions. Fig.10 shows the half-width of angular distribution of secondary ions after acceleration. It is seen that the half-width decreases with acceleration, and that the effect is largest at low incident atom energy.

Fig.11 shows ($\Delta\phi/\Delta\phi_{acc}$), the ratio of the angular half-width of secondary ions at the entrance to the analyzing magnet, without and with acceleration respectively, plotted against energy of incident atoms. Squares show the deduced ratio from measurements shown in fig.9 and fig.10. The dotted line represents $(\Delta\phi/\Delta\phi_{acc}) \propto (1/E_{//})^{0.5}$, where $E_{//}$ is the total forward energy of the secondary ions, and $E_{//} = (E_{atom} + U_{acc})$, the sum of incident atom energy plus the acceleration gain. It is seen that the measured increased focusing of the secondary ions follows this simple model. This result has been used in modeling the ion trajectories after the stripping foil.

c) Modeling of ion trajectories in magnetic and electric fields

To optimize the dispersion system a numerical model for ion motion in the electric and magnetic fields of ISEP was developed. The code calculates the fields and traces the ion trajectories in 3-D. The field sources may be constant currents, or magnetic elements with both linear and non-linear dependence of B and H. For electric fields, conductors with fixed potentials and dielectrics are used. The magnetic field is calculated using finite spatial elements method for non-linear B(H) dependence and finite surface elements method otherwise. Electric field is calculated using finite surface elements method. Up to three symmetry planes or rotation symmetry can be introduced to increase the computation speed. The modified Runge-Kutt method is implemented to calculate the ion trajectory. The code puts no limitation on system geometry. The purpose of the calculation was to optimise the parameters of stripping/acceleration/focusing and magneto-electric dispersion systems to allow the ions to reach the detector with minimal losses and suitable focusing. This results in maximal detection efficiency for H, D and T atoms entering the ISEP.

(d) Optimisation of the ISEP layout

The numerical code described above together with experiments on scattering in the stripping foil and on beam divergence after acceleration give us the possibility to model ion trajectories. In the

modelling we took into account measured angular distribution, as shown in fig.6, and the experimental result that increase in ion velocities due to acceleration can be added to their primary velocities. The goals of ISEP optimisation using numerical simulation were to obtain (1) two-dimensional focusing in the magnetic field and to minimise ion losses in the magnet gap by adjusting the magnetic field geometry. (2) good mass separation and minimal losses of H,D and T ions in electric field located between the magnetic field and the detectors by adjusting electric field geometry. (3) good focusing of the ions at the entrance to the detectors and to define exactly the location of H, D and T detectors shown in fig.3.

Fig.12 presents the result of optimisation of ISEP layout found using the numerical modelling described above. The ion trajectories shown correspond to ISEP Setup#1, which is conceived for measuring the deuterium-tritium composition of JET DT plasmas. Discussion of Setup #1 later gives the required magnetic field, condenser and acceleration voltages. The detectors are located in a plane where the trajectories achieve sufficient two-dimensional focusing to give most detection efficiency with least cross-talk($\leq 10^{-2}$) between ions of neighbouring masses. Dispositions of detectors in the detector plane are shown in fig.3.

In order to obtain good focusing it was necessary to use specially shaped non-uniform magnetic and electric fields. The non-uniform magnetic field was obtained by use of non-uniform gap between magnet poles shown in fig.12. The two-dimensional shape of the condenser shown in fig.12 produced non-uniform electric field. Fig.13 shows the measured and modelled magnetic field in the ISEP. The observed close agreement between the two validates the model.

5. CALIBRATION OF ISEP USING ATOMIC BEAMS, AND BENCH-MARKING OF A NUMERICAL MODEL OF ISEP PERFORMANCE.

Extensive measurements and calibrations were carried out to establish the following key parameters of the ISEP, and to bench-mark a numerical model for ISEP performance, which incorporates stripping, scattering, secondary ion acceleration, and electromagnetic dispersion:
(a) Exact ion energy E_n and ion mass measured at the 32 channels of the analyzer, (b) energy widths ΔE_n of the channels, and (c) detection efficiency for H, D and T atoms at the 32 ISEP detectors. To this end we have used a calibration facility producing hydrogen and deuterium atomic beams with known energy and intensity, in the energy range $5 \leq E_{H^0, D^0}(\text{keV}) \leq 27$ keV. This data was used to benchmark a model with which to extrapolate the calibration to higher energies, and to tritium atoms. The model incorporates all the primary processes occurring in analysis and detection of H, D and T atoms. The five processes are as follows:

(1) Stripping efficiency of the thin(300) carbon foil. Fig.14 presents, as function of ener gy of hydrogen atoms incident on the foil, the equilibrium fractions of hydrogen atom fragments emerging from the foil, integrated over all scattering angles, published in ref.[11].
(2) Energy loss suffered by the secondary ions straggling through the 300≈ carbon foil. This was calculated using the numerical model described in ref.[9,10]. Testing our calculation

yields that a 5 keV hydrogen atom loses ~2.6keV and a 100keV atom loses ~4keV. These results are in good agreement with existing experimental data, thus validating our calculation.

(3) Scattering of the secondary ions after stripping. We have used our experimental results shown in fig.5 and calculations described in ref.[9,10].

(4) Focusing effect of ion acceleration after stripping, as presented in figures 8—10.

(5) Trajectory modelling for ions going through the magnet gap and analyzing condenser, as described above in sections 4(c) and 4(d).

Calibrations using the atomic beams were used to benchmark the model. Note that the energy range of the actual calibration, $5 \leq E_{H^0, D^0}(\text{keV}) \leq 27$, is the most critical in respect of ion energy loss and scattering in the stripping foil. Modelling here is not so reliable as at higher energies where the influence of ion energy loss and scattering is relatively small. Therefore validating the model of ISEP performance using experimental data in the low energy range is of crucial importance. For reasons given before ISEP calibrations for tritium have been extrapolated using the measured deuterium data and modelling, taking into account that according to theoretical predictions [9,10] and measurement (fig.6), there is not a substantial difference in scattering for H^+ and D^+ ions. We therefore assume that there is not a substantial difference in scattering of T^+ ions either. In Tables I→IV below we present set-up parameters for four ISEP set-ups. The chosen set-ups are optimised for different applications, as described in the caption for each table. The corresponding full calibration data, measured and modelled where necessary, are presented for Table I, showing the energy E(keV) of atoms detected in 14 channels assigned to H, 10 channels to D, and 8 channels to T atoms. Corresponding values for the percentage channel width $\Delta E/E(\%)$, and channel efficiency K(E) are also given. For conciseness Tables II→IV give only the channel energies, however full calibration data including $\Delta E/E(\%)$ and K(E) is available for all the set-ups listed. Moreover, new set-ups can be calculated when required.

Table I

U_{acc} = 80 kV
B = 3.636 kG
$\pm U_c$ = 8.22 kV

Column Number	H-row E_H(keV) | ΔE/E(%) |K(E)			D-row E_D(keV) | ΔE/E(%) |K(E)			T-row E_T(keV) | ΔE/E(%)| K(E)		
1	26.1	11.3	0.224						
2	38.3	9.8	0.385						
3	50.1	8.4	0.486						
4	62.0	8.1	0.561						
5	77.5	7.3	0.64						
6	92.1	6.6	0.7	5.8	22.9	0.0263			
7	105	6	0.745	13.4	17.5	0.0966			
8				20.5	13	0.14			
9	131	5.2	0.83	27.6	11	0.174			
10				34.5	9.5	0.219			
11	158	4	0.881	41.7	8.1	0.256			
12							5.0	23.3	0.018
13	191	3.4	0.92	58.5	5.3	0.32	12.0	14	0.0526
14							19.1	11	0.0762
15	230	2.8	0.965				26.4	8	0.0972
16	--			87.5	4.2	0.414	32.7	7.3	0.116
17	270	2.3	0.98				40.3	6.3	0.142
18	340	1.9	1.0	133	2.7	0.568	63.7	4.3	0.219
19	430	1.5	1.0	178	1.9	0.674	93.7	2.8	0.287

JG02.359-1c

Setup #1: D/T thermal set-up suitable for determining the spatial profile of n_D/n_T in JET DT plasmas. Modelling of atomic flux emitted by the plasma [6] shows that the energy range chosen corresponds to the atomic source functions located from the plasma core to the edge. Acceleration voltage U_{acc}, analyzing magnetic field B and analyzing condenser voltage $\pm U_c$ are given at the top of the table. The table presents the energy E(keV) of H, D and T atoms detected, the percentage energy width ΔE/E(%) and detection efficiency K(E) of the channels.

Table II

U_{acc} = 10 kV
B = 1.35 kG
$\pm U_c$ = 1.10 kV

Column Number	H-row E_H(keV)	D-row E_D(keV)	T-row E_T(keV)
1	4.8		
2	6.5		
3	8.2		
4	9.9		
5	12.1		
6	14.2	--	
7	15.9	--	
8		--	
9	19.5	5.0	
10		6.0	
11	23.2	7.0	
12			--
13	27.6	9.4	--
14			--
15	32.7		4.8
16		13.5	5.7
17	38.0		6.8
18	46.8	19.8	10.1
19	58.2	25.8	14.4

JG02.359-3c

Setup #3: H/D thermal set-up suitable for determining spatial profile of n_H/n_D in a deuterium plasma with hydrogen minority. Low acceleration voltage here is sufficient because the neutron/γ-ray background is expected to be small for such plasmas.

Table III

U_{acc} = 0 kV
B_{Hall} = 4.13 kG
$\pm U_c$ = 11.1 kV

	H-row E_H(keV)	D-row E_D(keV)	T-row E_T(keV)
1	152		
2	169		
3	185		
4	203		
5	225		
6	246	126	
7	264	135	
8		144	
9	302	154	
10		163	
11	341	174	
12			125
13	389	197	133
14			143
15	446		152
16		239	161
17	506		172
18	606	305	205
19	738	370	248

JG02.359-3c

Setup #4: ICRF minority set-up suitable for measurements of ICRF driven hydrogen minority ion energy distribution in deuterium plasmas. Zero acceleration voltage can be used here because neutron/ γ-ray background is expected to be small in this JET regime. Moreover the absence of acceleration gives access to a very wide energy range required for this application.

Table IV

U_{acc} = 20 kV
B_{Hall} = 1.82 kG
$\pm U_c$ = 2.0 kV

Column Number	H-row		D-row		T-row	
	E_H(keV)	$\Delta E/E$(%)	E_D(keV)	$\Delta E/E$(%)	E_T(keV)	$\Delta E/E$(%)
1	4.2	29				
2	7.0	17.3				
3	9.9	14				
4	12.9	12				
5	16.8	10.5				
6	20.5	8.9	--	--		
7	23.6	8.3	--	--		
8			--	--		
9	29.9	7	5.0	24		
10			6.6	17		
11	36.2	5.9	8.4	14		
12					--	--
13	43.8	5	12.7	8.8	--	--
14					--	--
15	52.5	4.1			4.8	20
16			19.8	5.8	6.6	13
17	61.5	3.8			8.3	10.5
18	76.7	3	30.9	4.3	14.1	6.7
19	97.0	2.5	41.3	3.7	21.6	4.8

JG02.359-4c

Setup #5: H/D thermal setup. This setup is suitable for determination of the hydrogen isotope composition n_H/n_D in typical JET deuterium plasmas with hydrogen minority, and with low DD fusion neutron production rate $S_n \times 5 \cdot 10^{15}$ n/s.

The energy widths ΔE of ISEP channels, as function of energy of incoming H and D atoms for set-ups #1, #2, #3 and #4 were measured using the atomic beam calibration facility, in the energy range 5≤E(keV)≤27 and supplemented with modelling at higher energies. Overlapping experimental and calculated data are in good agreement. For tritium where measurements are not available we use only the modelling data. Fig.15 (a, b) show the energy dependence of ΔE/E for D^0 and T^0 atoms in Setup #1. Below is a summary of typical behaviour of ΔE for the set-ups listed above.

Setup #1: for D^0 in the energy range (5.8 — 178) keVΔE/E decreases monotonically from 22% to 2%, while for T^0 in the range (5.0 — 93.7) keV
ΔE/E decreases from 23% to 2%.
Setup #2: for H^0 in the range (4.8 — 58.2 keV)
ΔE/E decreases from 12.5% to 2%, while for D^0 in range (5.0 — 25.8) keV
ΔE/E decreases from 10.0% to 3%.
Setup #3: for H^0 in range (152 — 738) keVΔE/E decreases from 4.0% to 1.7%, while for D^0 in range (126 — 370) keVΔE/E decreases from 3.5% to 1.7%.
Setup #4: Table IV above gives tabulated values for ΔE/E for H, D, and T atoms

For applications enumerated in the introduction, an instrument capable of measurement with high contrast between neighboring masses is required. Mass rejection of ISEP was also measured using the calibration facility. We require to know the mass rejection M_r, which is the fraction of ions of mass m_2 leaking into a detector of ISEP designated for measuring ions of mass m_1, when flux of only ions of mass m_2 is presented to the ISEP. Referring to fig.3, modeling suggests that in ISEP the most critical situation in respect of mass rejection occurs between deuterium channel #7 (D7) and tritium channel #2 (T2), because T2 is located directly above D7. Similarly between hydrogen channel #6 (H6) and deuterium channel #1 (D1). Magnitude of mass rejection M_r was measured using a deuterium atomic beam. Then M_r(D7/T2) = C(D7)/C(T2), the ratio of count rate registered by detectors D7 and T2 when a purely deuterium flux is presented to ISEP. The result is $M_r(D_7/T_2) \sim 10^{-3}$, and similarly $M_r\,(H_6/D_1) \sim 10^{-5}$. From this we conclude that the mass rejection of ISEP is not less than $\sim 10^3$ for any combination of D and T detectors, and not less than $\sim 10^5$ for any combination of H and D detectors.

The absolute detection efficiency K(E) of ISEP, for H, D and T atoms as function of energy of atoms, for the different set-ups listed previously, was determined by measurement and modeling. The results are shown in figs. 16, 17 and 18, where the solid circles show measured K(E) and the dashed curve shows result of modeling for K(E). The solid curve in the figures shows the equilibrium fraction of H^+, D^+ and T^+ ions emerging from the carbon stripping foil, data taken from fig.14 and reduced by factor 0.9 to account for transparency of the nickel mesh supporting the carbon foil. The difference between the measured or modeled K(E) and the equilibrium fraction of Figures 16(a) and 17(a, b) show that there is good agreement between measured and modeled values of detection

efficiencies K(E) for H and D atoms in the calibration range 5≤E(keV)≤27. This allows the possibility of extrapolating K(E) to higher energies using the modeling. We see that at relatively low energies (Setup 1# and Setup #2) the measured values of K(E) are lower, by a factor 2~3, than those predicted for the corresponding ion equilibrium fractions after the stripping foil. This is connected with strong scattering resulting in ion losses. In the high energy range (for Setup #3 shown in fig.18(a, b)) we see that for atoms of energy E > 150keV the scattering is not important any more and the ISEP detection efficiency is limited only by the equilibrium fraction of ions emerging from the stripping foil.

6. RESULTS OF FIRST APPLICATION OF ISEP FOR MEASUREMENTS OF HYDROGEN MINORITY DEUTERIUM PLASMAS IN JET

ISEP was installed, tested and commissioned on JET in the summer of 2000. In this section we present first results of ISEP application for measurement of Ohmic, ICRF and NBI heated deuterium plasmas. Fig.19 shows the measured energy distribution of efflux of H and D atoms from a low density low temperature ohmic heated plasma, using Setup #5 shown in Table IV above. The measured absolute line-of-sight integrated energy distribution of atomic efflux, $\overline{\Gamma}(E_i)$, to the ISEP is determined using the expression:

$$\overline{\Gamma}\,(\mathrm{E_i})\ (\mathrm{m^{-2}\,s^{-1}\,keV^{-1}\,st^{-1}}) = \frac{\mathrm{N^{+}\,(E_i)}}{\Delta \mathrm{E_i} \times \Delta \mathrm{t} \times \mathrm{K\,(E_i)} \times (\mathrm{S\Omega})}$$

The index i = 1→32 represents the ISEP channel number, where channels i = 1→14 receive H ions, i = 15→24 receive D ions, and i = 25→32 receive T ions, $N^{+}(E_i)$ is the number of secondary ion counts registered in the ISEP channel(i), ΔE_i is the energy width of the channel, Δt is the integration time used, $K(E_i)$ is detection efficiency for the atoms, and $(S\Omega)$ is the Øtendue of the ISEPcollimator. The present installation on JET gives $(S\Omega) = 5.2 \times 10^{-6}\,\mathrm{m^2}$ st. The time resolution of the measurement is limited by the scintillator decay time of $\tau \approx 2.5\mu s$. If maximum permissible secondary ion count rate of 2×10^5 /s were obtained in an experiment then a minimum measurement time resolution of $\Delta t = 1.5ms$ would be possible with the present installation on JET. In fig.19 the data for hydrogen channel #1 corresponds to count rate of ~500/s, and that for deuterium channel #1 to ~3000/s.

Fig.19 shows also a comparison between measured and modeled $\overline{\Gamma}(E_i)$. The numerical modeling of efflux, making use of measured plasma parameters, is fully described in ref.[6]. In detail the modeling is based on solution of a kinetic equation for transport of atoms in the plasma. Input of radial profiles of ion and electron temperatures and of electron density are required for the modeling. The principal unknown in the modeling is the absolute density of thermal hydrogen isotope atoms in the plasma, these thermal atoms are the main agents of CX reactions giving the efflux. In the modeling we have assumed that (a) the plasma ion energy distribution functions were Maxwellian, (b) the ion temperatures $T_i(r)$ of the two ion species were equal everywhere, and (c)the spatial profiles of ion temperature were the same as the measured electron temperature. Since the ion temperature and its spatial profile were not measured, $T_i(0)$ = 1.95 keV was obtained by iteration to get the best fit between measured and modeled $\overline{\Gamma}(E_i)$. By ascribing a temperature to the atomic

efflux, $T_i(0) \cong 1.9$ keV may also be deduced directly from the slope of measured energy distribution of $\overline{\Gamma}(E_i)$. Applications of ISEP require careful consideration of all assumptions (a, b, c) made above. Sensitivity of the modeled efflux to the assumptions is fully analyzed in ref.[6]. The modeling code calculates also an emissivity function ε(r,E) for efflux of atomic hydrogen and deuterium from the plasma. Fig.20 presents modeled ε(r,E) for different energies spanning the energy range of efflux shown in fig.19.

Providing the assumptions (a, b, c) given above are valid, then from fig.19 we infer that the measured $\overline{\Gamma}(E_i)$ for the two isotopes is close to the modeled one. The only adjustable normalization factor is the absolute density of hydrogen isotope atoms in the plasma. Normalization of modeled and measured $\overline{\Gamma}(E_i)$ allows us to determine the ratio of the hydrogen isotope ion densities in the plasma, as explained in detail in ref.[6]. Fig.20 shows that for these plasma conditions H and D atoms of 20 keV are emitted from the plasma core. ε(r,E) for atoms with lower energies are shifted toward the outside, illustrating the method by which the radial profile of relative hydrogen isotope composition of the plasma may be deduced from such measurements. Measurements and modeling shown in fig.19 and fig.20 yield the hydrogen isotope composition of this plasma, $n_H/n_D(0 \le r/a \le 0.5) = 0.07$. Statistical errors on this result are small, but large systematic errors could arise due to the assumptions made in deducing this result, as discussed fully in ref.[6].

Fig. 21 shows measured $\overline{\Gamma}(E_i)$ for D and H atom efflux from a high density deuterium plasma heated to high ion temperature by NBI, pulse #52246 at t(s) = 57.5-58.5. We see that $\overline{\Gamma}(E_i)$ is much greater in this pulse than from the low density low ion temperature plasma of pulse #52010 (fig.19). Here the secondary ion count rate is $\sim 9.3 \times 10^3$/s for hydrogen channel #1 and $\sim 5 \times 10^4$/s for deuterium channel #1. The curves in fig.21 show the modeled $\overline{\Gamma}(E_i)$ for H and D atoms, with the same assumptions (a, b, c) made above about ion energy distribution functions, the two ion temperatures and their profile shape. The modeling curves were determined by iteration to obtain best match between the measured and modeled H and D efflux, giving $T_i(0) = 15$ keV. The match is good for H atoms up to 60keV, whereas the measured D atom efflux begins to deviate from modeling above 30keV. This deviation corresponds to the non-Maxwellian slowing-down distribution of D ions due to deuterium NBI heating. Fig.22 presents modeled ε(r,E) for H and D atoms of different energies, for conditions of fig.21. It is seen that most of the atoms in the measurement energy range are emitted from the intermediate region $0.5 \le r/a \le 1$, with the maximum in ε(r,E) of 60keV atoms located at r/a~0.5. The efflux of atoms at higher energies was accurately measured, but the strong influence of NBI on measured deuterium energy distribution function precluded inference of n_H/n_D in the plasma core. The measurements shown in fig.21 and modeling yield the result $n_H/n_D(r/a \ge 0.7) = 0.1$ for the relative hydrogen isotope composition of this plasma. Herein lies the principal experimental challenge in extending the spatial range of the n_H/n_D determination, to devise a strategy for measurement of high energy atoms emitted from the core of a high density high temperature plasma in which the energy distribution functions of the ions can be approximated by Maxwellians. ISEP was used also for measurement of $\overline{\Gamma}(E_i)$ of energetic atoms during ICRF heating of hydrogen

minority ions in deuterium[D(H)] plasmas, using Setup #3 with zero accelerator voltage. Due to intrinsic high energy of H and D atoms emitted by such plasmas, falling into regime of high detection efficiency of ISEP, secondary ion acceleration was not necessary. Also because neutron/γ-ray background is usually small in such plasmas. Moreover absence of acceleration gives a wide dynamic energy range for the ISEP required for such measurements. Fig.23 shows measured $\overline{\Gamma}(E_i)$ for high energy H and D atom efflux.

This kind of measurement is required in ICRF heating experiments to infer evolution of ion energy distribution and the tail temperature . To infer the energy distribution function of ions in the plasma from these measurements, it is necessary to invoke the mechanism of plasma ion neutralization, for which there are many agents. The required neutralization model was developed in ref.[7], quantitatively validated and widely applied in JET to measure and interpret different aspects of energetic ion dynamics.

7. CONCLUSIONS

A Neutral Particle Analyzer/Isotope Separator (ISEP) for measurement of spatial distribution of relative hydrogen isotope composition of JET plasmas has been developed at the A.F. Ioffe Institute in St.Petersburg, Russia. The engineering design of ISEP was developed and implemented in collaboration with the JET Joint Undertaking. The instrument can be regarded as a prototype of that required for measurement of $n_D(r)/n_T(r)$ in ITER plasmas, and the instrument parameters and design features are specifically chosen for this purpose. The main features of the ISEP are: (1) use of a thin carbon foil for reionization of the incident atoms, thus eliminating gas cells and gas sources of conventional NPAs, (2) acceleration of the secondary ions after stripping in order to access regime of higher detection efficiency of the NPA, and to better separate ion pulses from neutron/γ-ray induced pulses in the scintillator detectors, (3) E//B analyzer with a specially designed non uniform magnetic and electric fields to give focussing, increased throughput and greater contrast between neighboring isotopes, (4) detectors consisting of thin CsI(Tl) scintillator attached to thin window photo-multiplier tubes giving very low sensitivity to neutron/γ-ray background, the ratio of ion to neutron/γ-ray sensitivities of $\geq 10^7$, (5) high mass separation, giving contrast between neighboring masses of more than 10^3, (6) high detection efficiency (close to 100% for the higher energy ions). First measurements on JET plasmas using the ISEP demonstrate well the capabilities of the instrument for studies of hydrogen isotope composition of the plasma and of energy distribution function of the isotope ions. Proposed future DT experiments on JET will test applications of the ISEP in deuterium-tritium plasmas. Further development of detectors to minimize, or even eliminate, the need for neutron/γ-ray shielding of the NPA on ITER seems feasible.

8. ACKNOWLEDGEMENTS

The authors are grateful to Misha Beldishevski and Clare Jenkinson for developing computer software for control and data analysis, and to Paul R. Thomas for much support in procuring ISEP and deploying it on JET. This work was performed partly under the framework of the JET Joint

Undertaking, and partly under the European Fusion Development Agreement. The UKAEA authors were funded jointly by the UK Department of Trade and Industry, and by Euratom.

9. REFERENCES

[1]. M. Bessenrodt-Weberpals, F. Wagner, and the ASDEX Team, Nuclear Fusion, **33,** 1205 (1993).

[2]. M. C. Zarnstorff, S. D. Scott, C. W. Barnes, R. Bell, C. E. Bush, et al., Proc. 15th IAEA Conference on Plasma Physics and Controlled Nuclear Fusion Research, Seville, Spain, 1994. Paper IAEA-CN-60/A2-2, Volume 1, IAEA Vienna 1995.

[3]. R. J. Hawryluk, H. Adler, P. Alling, C. Ancher, H. Anderson, et al., Physical Review Letters **72,** 3530 (1994).

[4]. D. F. H. Start, J. Jacquinot, V. Bergeaud, V. P. Bhatnager, G. A. Cottrell, et al., Physical Review Letters **80,** 4681 (1998).

[5]. P. R. Thomas, P. Andrew, B. Balet, D. Bartlett, J. Bull, et al., Physical Review Letters **80,** 5548 (1998).

[6]. V. I. Afanasyev, A. Gondhalekar and A. I. Kislyakov, On the Possibility of Determining the Radial Profile of Hydrogen Isotope Composition of JET Plasmas, and of Deducing Radial Transport of the Isotope Ions. JET Report JET-R(00)04, 2000. The report is available at the Institute of Physics, London, Website http://www.iop.org/Jet/article?JETR00001&JETR00004

[7]. A. A. Korotkov, A. Gondhalekar and A. J. Stuart, Nuclear Fusion **37,** 35 (1997).

[8]. A. I. Kislyakov, A. V. Khudoleev, S. S. Kozlovskij and M. P. Petrov, Fusion Engineering and Design, **34-35,** 107 (1997).

[9]. J. F. Ziegler, J. P. Biersack and U. Littmark, *The Stopping and Range of Ions in Solids,* (Pergamon Press, New York, 1985).

[10]. J. P. Biersack and L. Haggmark, Nuclear Instruments and Methods, **174,** 257 (1980).

[11]. S. K. Allison, Review of Modern Physics, **25** 779 (1953), and Review of Modern Physics, **30,** 1137 (1958).

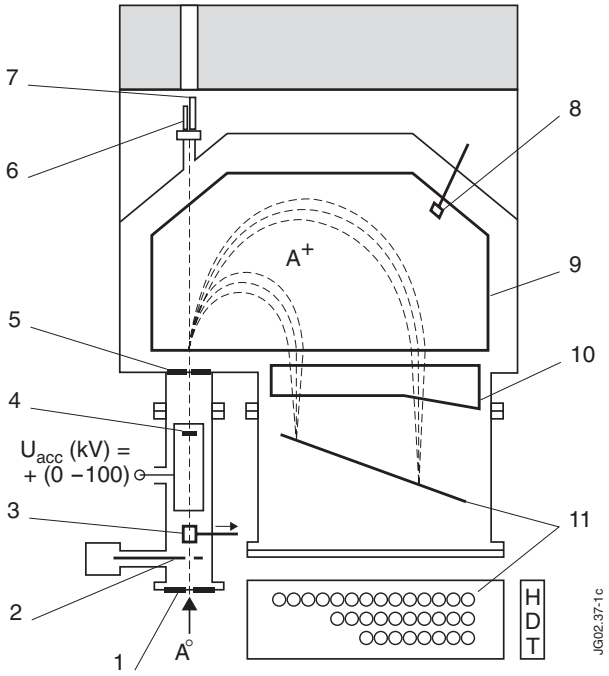

Figure 1: The ISEP layout showing the input aperture (#1), adjustable collimator/slit mechanism (#2), calibration aid (#3), stripping foil (#4), output aperture (#5), a light emitting diode (#6), alignment laser (#7), Hall probe (#8), electromagnet (#9), electrostatic condenser (#10), and the detector flange (#11) with 32 scintillator/PMT detector assemblies.

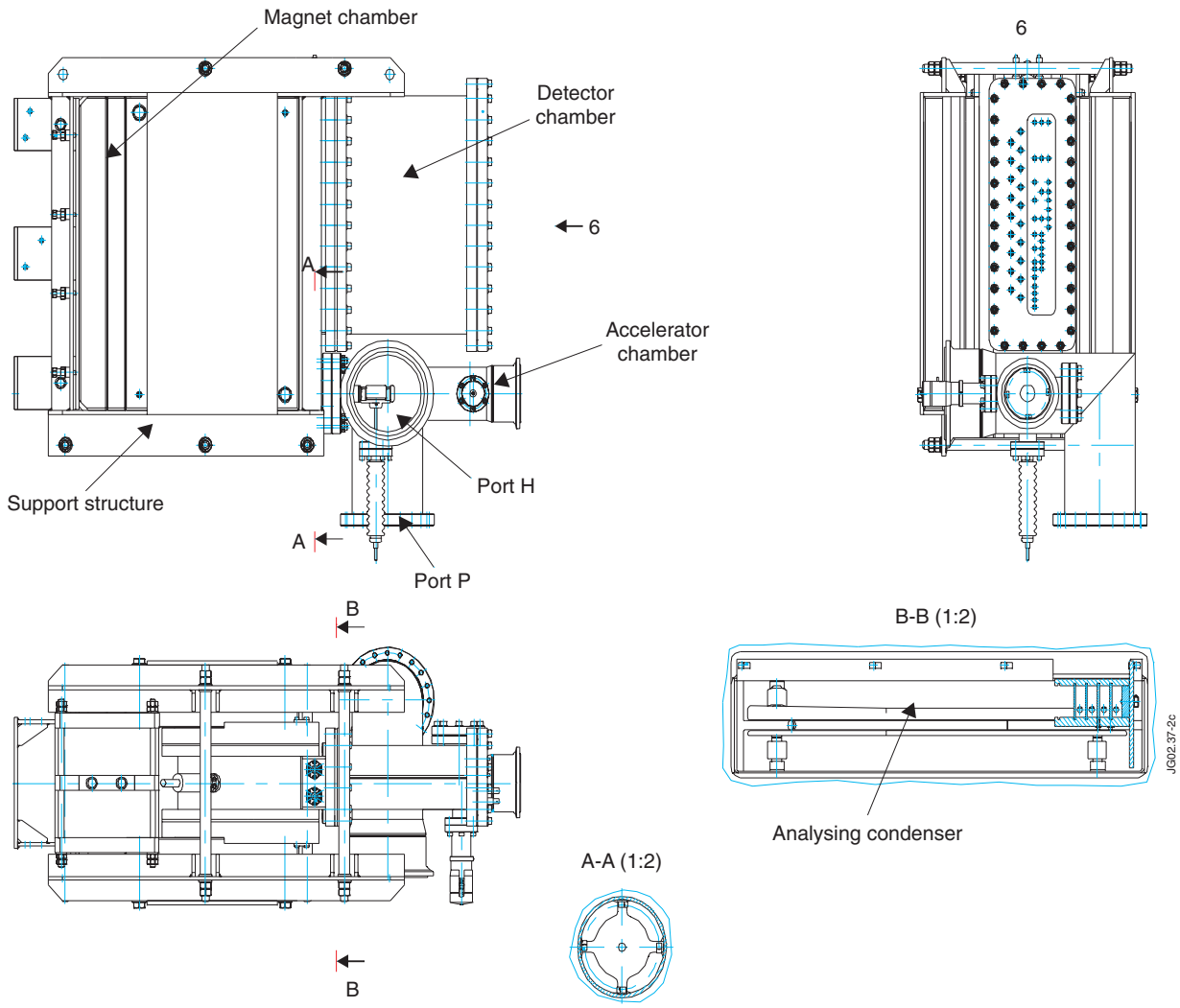

Figure 2: External view showing details of ISEP construction.

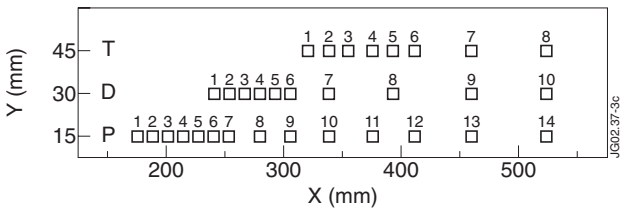

Figure 3: A view of the detector plane, showing three rows of detectors for the three different hydrogen isotope ion species. The detectors are arranged in nineteen columns, all detectors in a column are energised by one power supply. The X-axis shows the distance from the left edge of the magnet, along the direction of magnetic dispersion. The Y-axis shows the distance from the midplane of the magnetic analyzer.

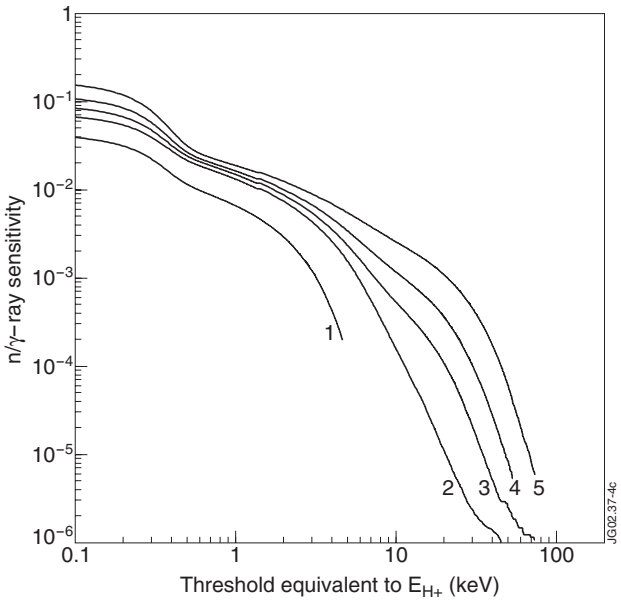

Figure 4: Results of laboratory tests of neutron/γ-ray sensitivity of the detectors, showing normalized counts in the ADC as function of pulse amplitude threshold, presented as equivalent hydrogen ion energy E_H (keV) . Curve #1 shows the sensitivity for a bare PMT, curves #2, #3, #4 and #5 show the sensitivity for the PMT with attached scintillator of respectively 1.1μm, 2.4μm, 4μm and 7μm thickness.

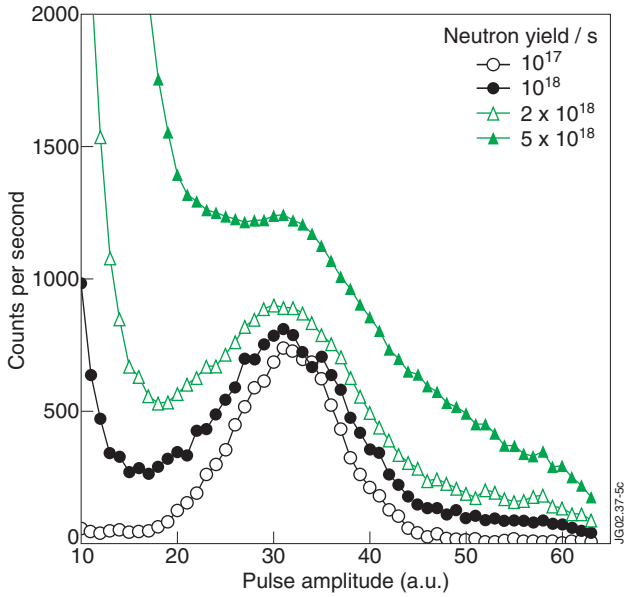

Figure 5: Model simulation of ISEP detector pulse height distribution when detecting D^+ ions in the presence of intense DT neutron background. Incident deuterium atom energy was taken to be E_d= 5keV, acceleration voltage U_{acc} = 8keV (total secondary ion energy E_D=85keV), D^+ count rate was 10^4/s, total neutron yield from the plasma was varied from 10^{17} to 5.10^{18} n/s.

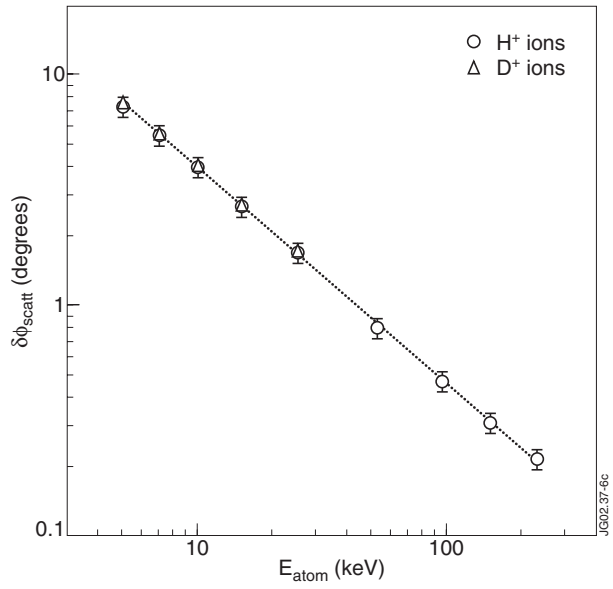

Figure 6: Variation of $\delta\phi_{scatt}$, the width of angular distribution of hydrogen and deuterium ions emerging from the 300 carbon foil, with ener gy of incident hydrogen and deuterium atoms.

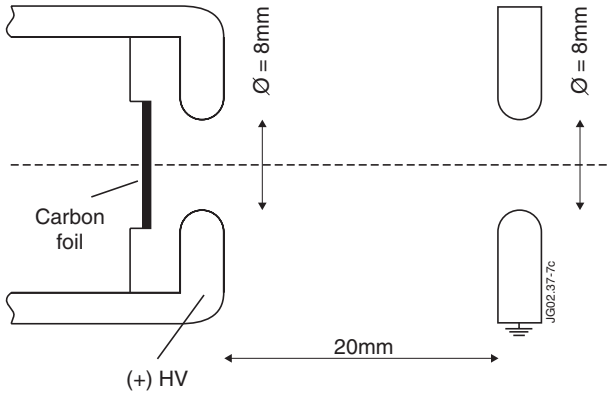

Figure 7: Accelerator electrode configuration to obtain optimal secondary ion focusing before injection into the analyzing magnet.

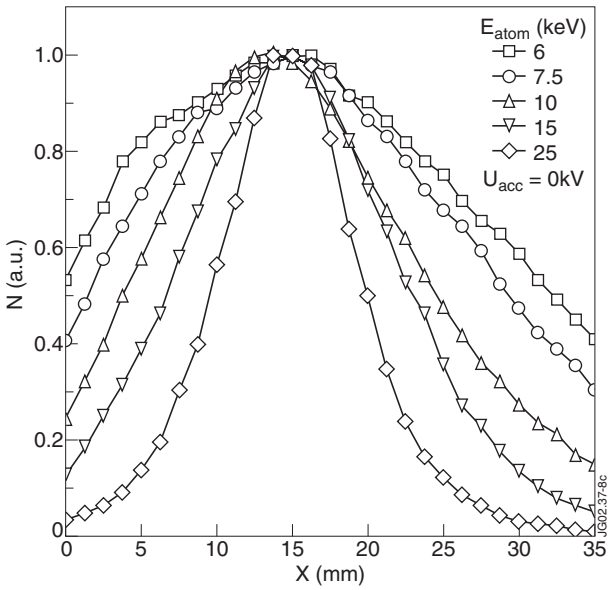

Figure 8: Spatial secondary H+ ion intensity distribution at the entrance to the analyzing magnet, in a direction perpendicular to the acceleration axis in the plane of magnetic dispersion, in the absence of secondary ion acceleration. X=14.5mm is the axis of the collimating apertures and accelerator.

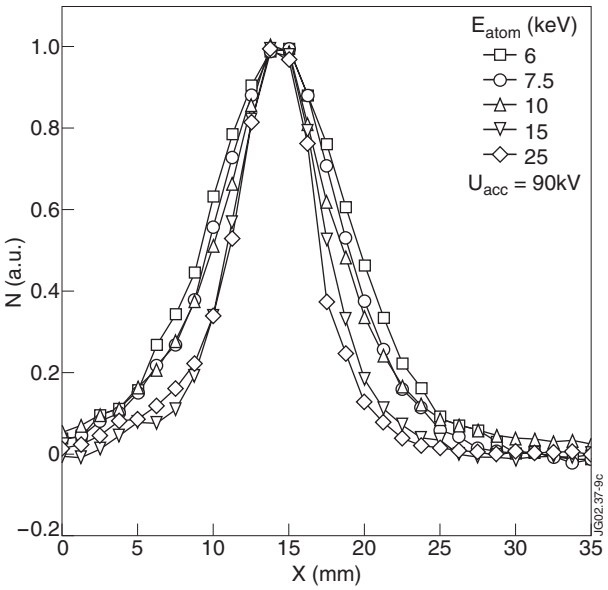

Figure 9: Spatial secondary H+ ion intensity distribution at the entrance to the analyzing magnet, in a direction perpendicular to the acceleration axis in the plane of magnetic dispersion, using acceleration voltage of 90kV. X=14.5mm is the axis of the collimating apertures and accelerator.

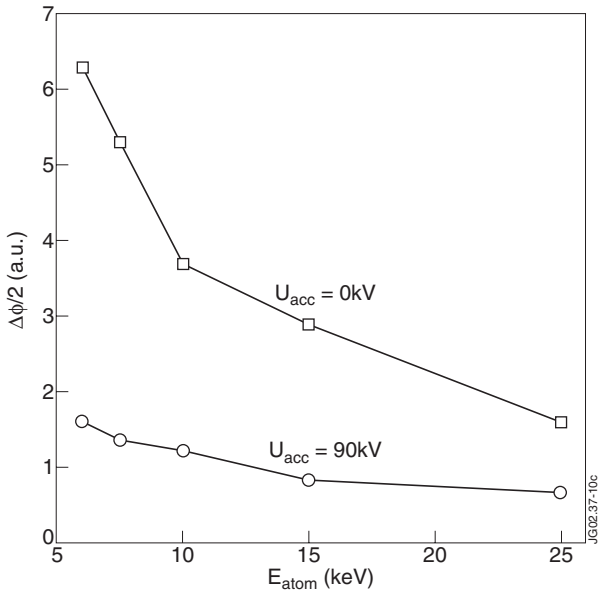

Figure 10: Comparison of half-width of angular distribution of secondary H+ ions, without(0kV) and with 90kV acceleration of the ions.

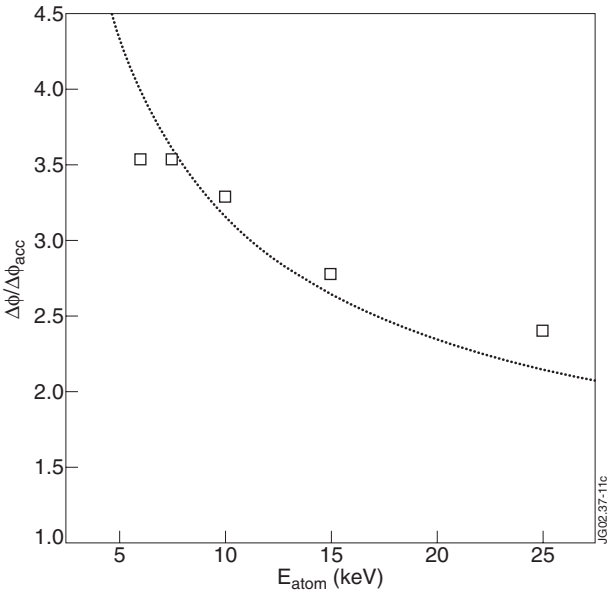

Figure 11: Ion focusing due to acceleration, expressed as ratio of angular half-width without and with acceleration ($\Delta\phi/\Delta\phi_{acc}$), as a function of incident atom energy. Squares show the experimental data, dotted line is a model variation ($\Delta\phi/\Delta\phi_{acc}$) $\propto \sqrt{(1/E_{//})}$.

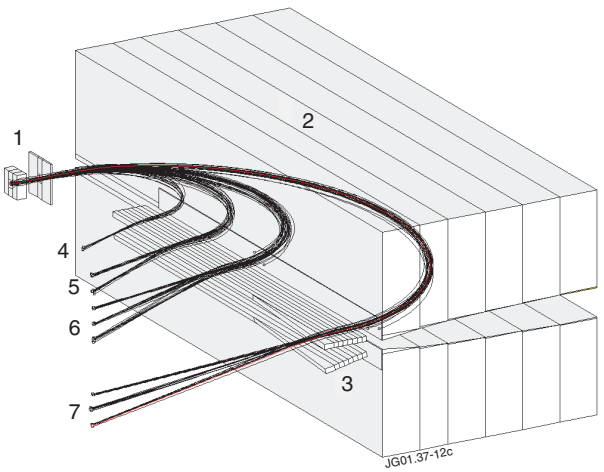

Figure 12: #1 is acceleration gap, #2 is analyzing magnet, #3 is electrostatic condenser, #4— #7 are ion trajectories of H(top), D(middle) and T(bottom) ions. Trajectories show: #4 H ions with E=26.1keV, #5 H ions (92.1keV) and D ions (5.8keV), #6 H ions (158keV), D ions (41.7 keV) and T ions (5keV), #7 H ions (430keV), D ions (178 keV) and T ions (93.7keV).

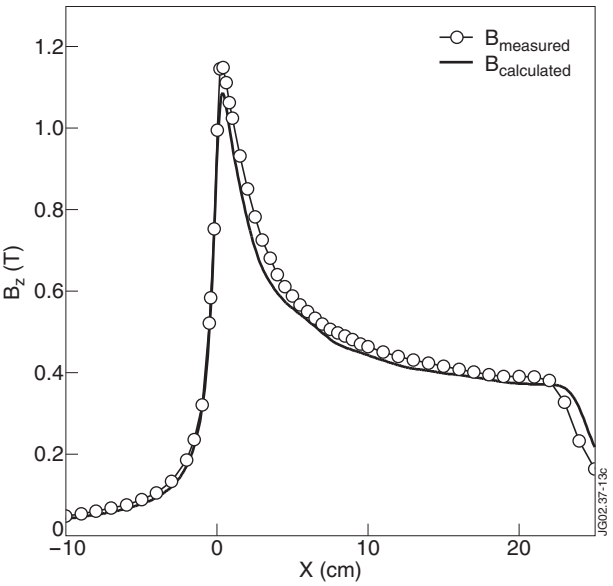

Figure 13: intensity of ISEP magnetic field B_Z outside and inside the magnet gap, measured along the input axis defined by the apertures #1, #2 and #5 shown in fig.1. The origin of the X-coordinate is at the entrance to the magnet gap, at aperture #5. Open circles show the measured field using a Hall probe. The solid line shows the model calculated magnetic field.

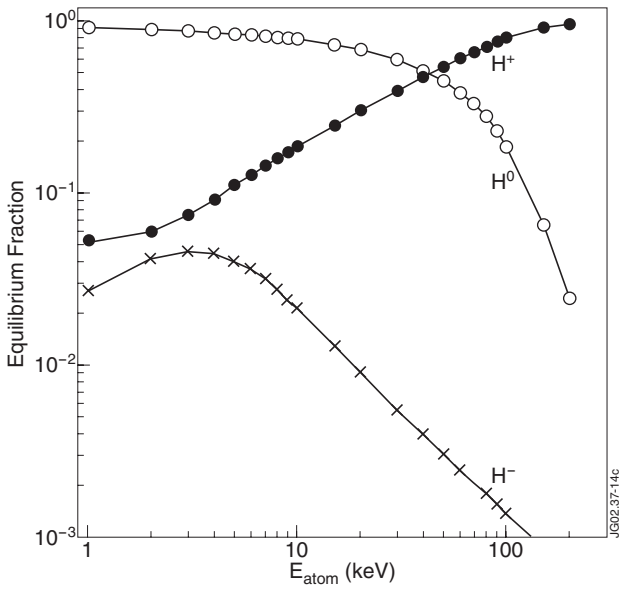

Figure 14: Equilibrium fraction of hydrogen atom fragments emerging from a 300≈ thick carbon foil, after a hydrogen atom is incident on it, integrated over all scattering angles.

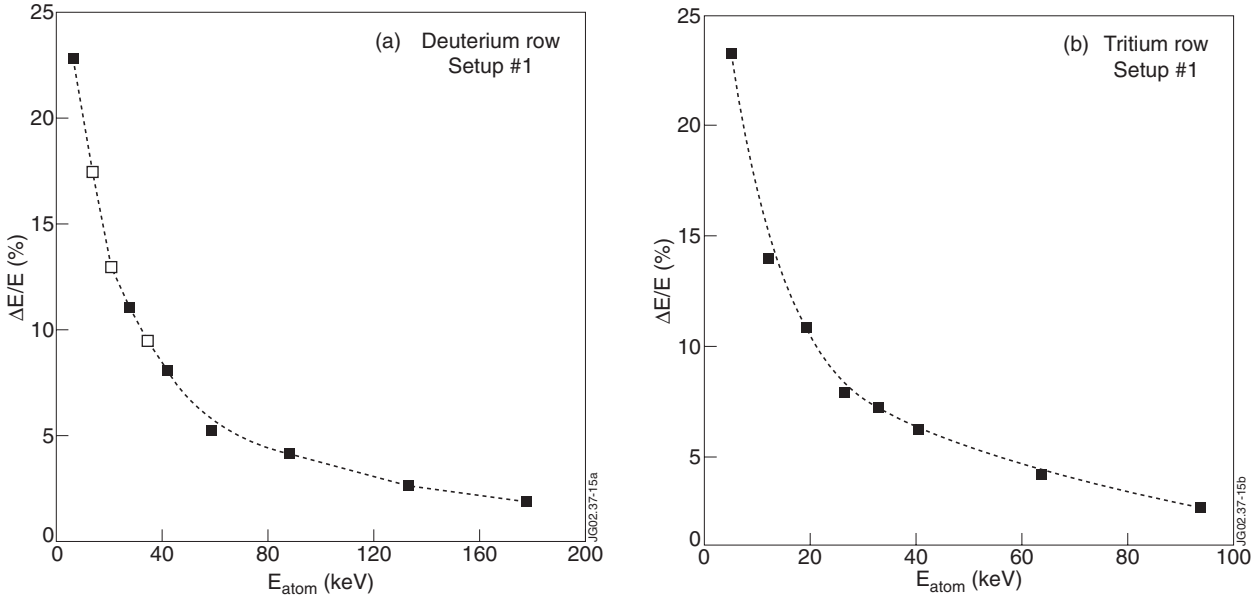

Figure 15: Relative energy widths ΔE/E of the ISEP channels for Setup #1, (a) for the deuterium detector row, where the open symbols show measured width and the closed symbols give the model calculated width, (b) for the tritium detector row, where all data is modeled.

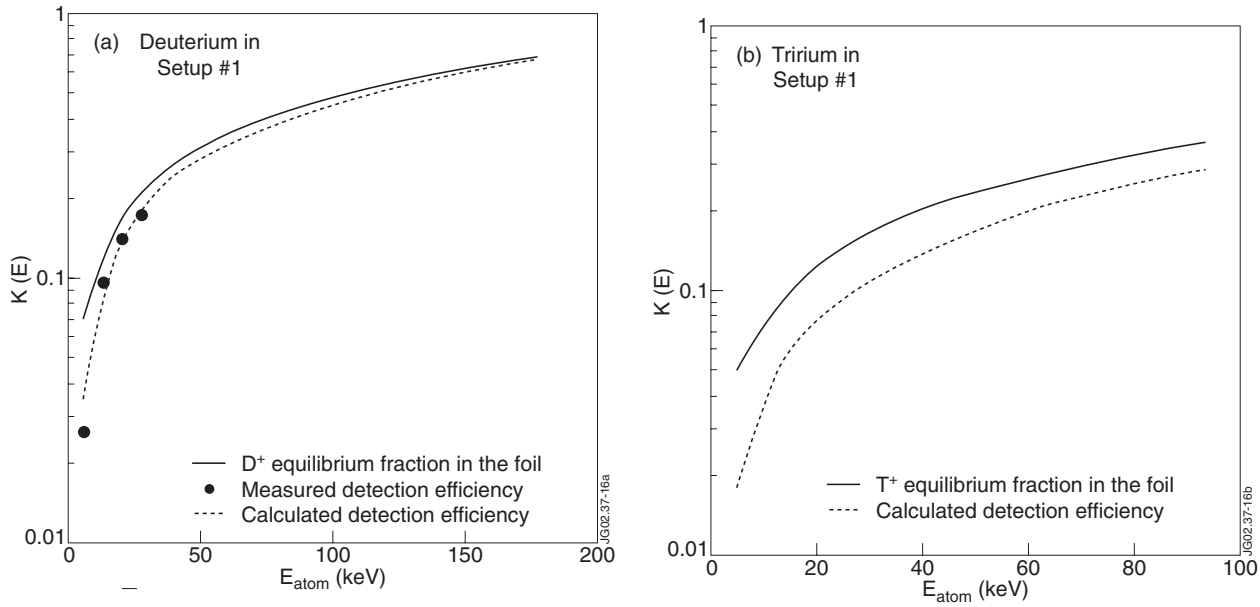

Figure 16: Detection efficiency K(E) for Setup #1 for D and T atoms, as function of atom energy. (a) shows the measured and modeled K(E) for D atoms, and modeled equilibrium fraction of D^+ ions emerging from the foil, whereas (b) shows modeled K(E) for T atoms and modeled equilibrium fraction of T^+ ions after stripping.

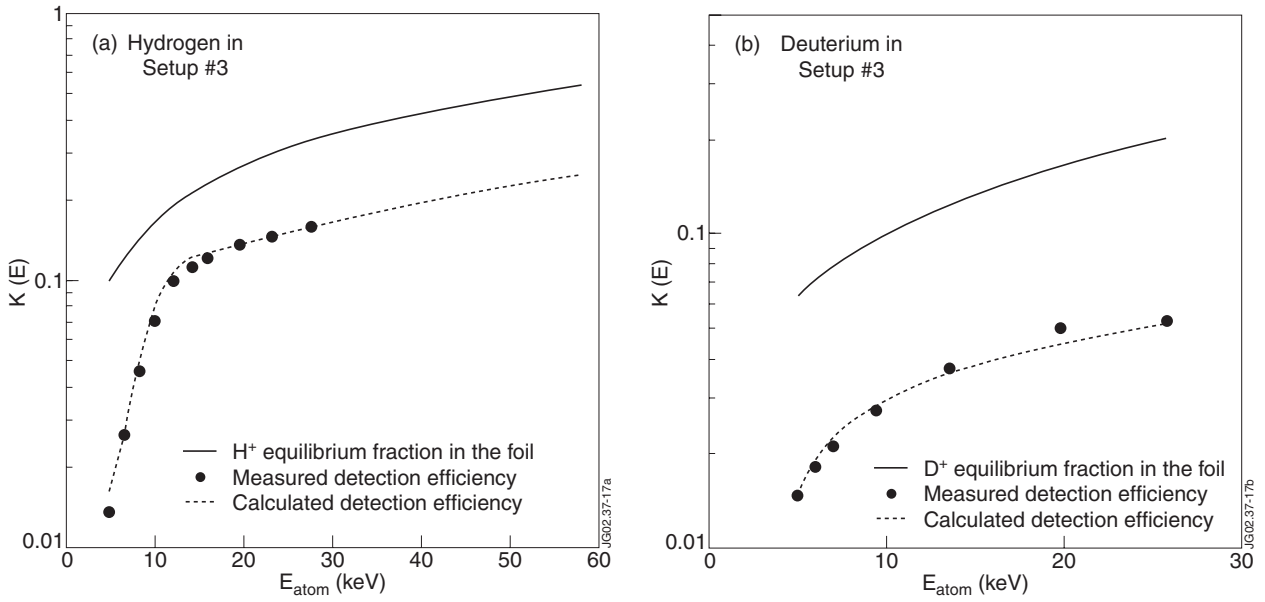

Figure 17: Detection efficiency K(E) for Setup #2 for H and D, as function of atom energy. (a) shows the measured and modeled K(E) for H atoms, and (b) shows measured and modeled K(E) for D atoms. The equilibrium fraction of H^+ and D^+ ions from the foil is also shown.

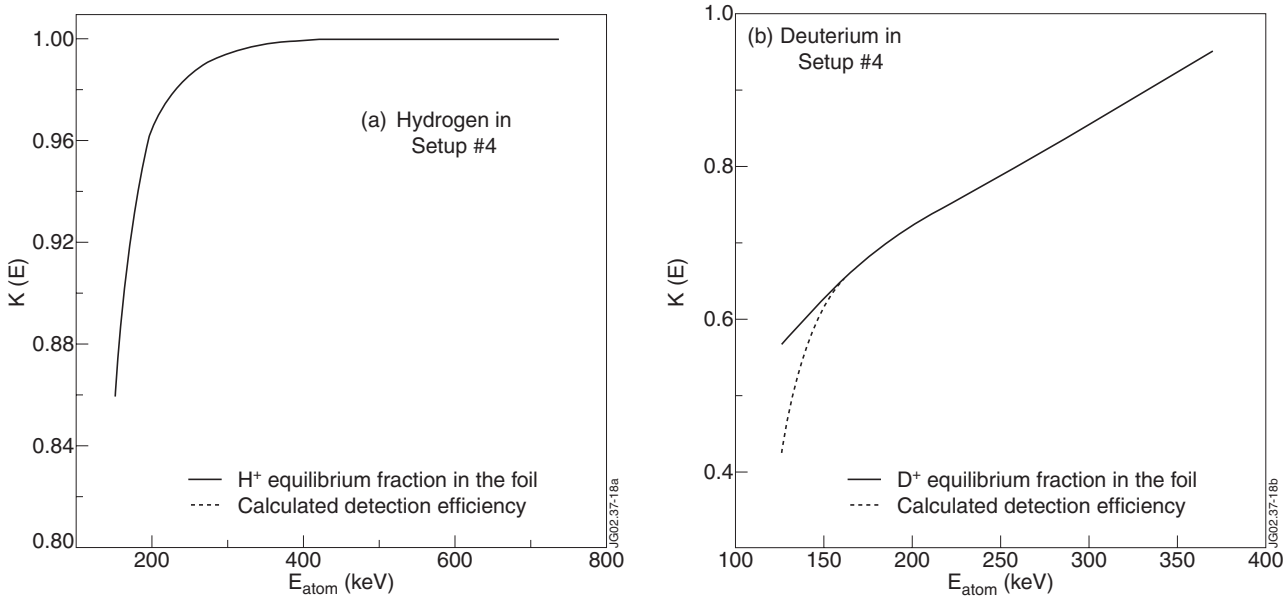

Figure 18: Detection efficiency K(E) for Setup #3 for H and D, as function of atom energy. (a) shows the modeled K(E) for H atoms, and (b) shows modeled K(E) for D atoms. In both figures modeled equilibrium fraction of H^+ and D^+ ions after stripping is shown.

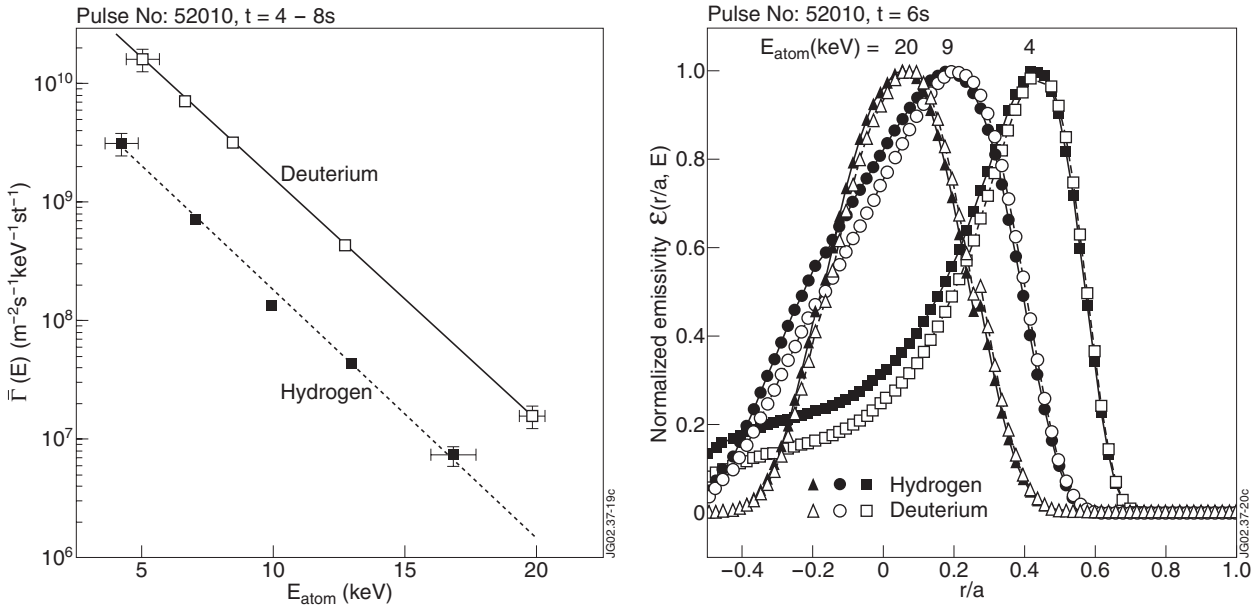

Figure 19: Line-of-sight integrated energy distribution function $\bar{\Gamma}(E)$ of H and D atomic efflux from an Ohmic heated plasma in Pulse No: 52010 averaged over 4-8s. Pertinent plasma parameters were: central electron density $n_e(0)=1.4.10^{13}$ cm^{-3}, central electron temperature $T_e(0)=3.06$ keV. Black and open squares are the measured effluxes of H and D atoms, and the dashed and solid lines show results of numerical modeling.

Figure 20: Modeled emissivity functions of H(solid symbols) and D(open symbols) atomic efflux for different energies, 20keV, 9keV, and 4keV, for Pulse No: 52010 at 6s. The emissivity function is plotted as function of normalized plasma minor radius (r/a).

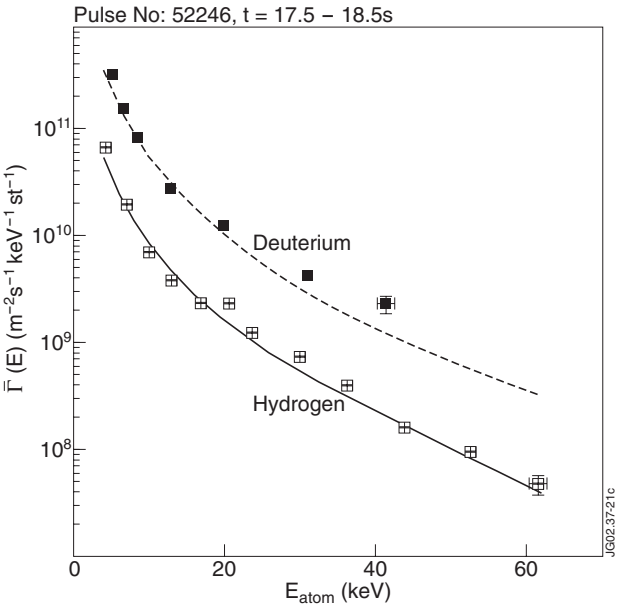

Figure 21: $\bar{\Gamma}$(E) for D and H atom efflux in Pulse No: 52246 at t(s) = 17.5-18.5. At the time central electron density and temperature were respectively $n_e(0)=9.6.10^{13}$ cm^{-3} and $T_e(0)$=5.06 keV. Deuterium NBI of P_{NBI} = 12.6 MW was employed. Solid and open symbols show measured efflux, and the dashed and solid lines are results of modeling.

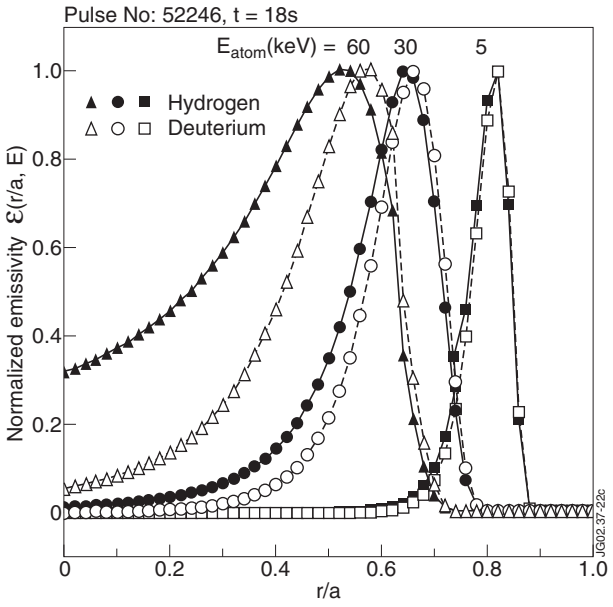

Figure 22: Calculated emissivity functions of H(solid symbols) and D(open symbols) atoms of different energies 60keV, 30keV and 5keV, forPulse No: 52246, plotted as function of normalized minor radius r/a. Plasma parameters were same as for fig. 21.

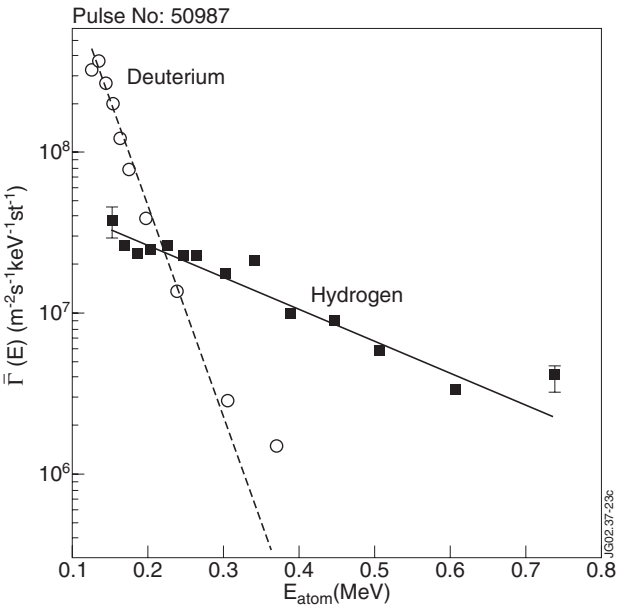

Figure 23: $\bar{\Gamma}$(E) for H and D atom efflux from a deuterium plasma in Pulse No: 50987, with 7MW of hydrogen minority ICRF heating and 7.6 MW of deuterium NBI heating.